Article

Online Adaptive Parameter Estimation of a Finite Control Set Model Predictive Controlled Hybrid Active Power Filter

Silvia Costa Ferreira [1,*] , João Gabriel Luppi Foster [2] , Robson Bauwelz Gonzatti [2,*] ,
Rondineli Rodrigues Pereira [2], Guilherme Gonçalves Pinheiro [2] and Bruno P. Braga Guimarães [2]

[1] Automatic Control Department, Federal University of Lavras, Lavras 37203-202, Brazil
[2] Institute of Engineering and Information Technology (IESTI), Federal University of Itajubá,
Itajubá 37500-903, Brazil; fosterelt@unifei.edu.br (J.G.L.F.); rondineli@unifei.edu.br (R.R.P.);
guilhermegpinheiro@unifei.edu.br (G.G.P.); brunoguimara@unifei.edu.br (B.P.B.G.)
[*] Correspondence: silvia.ferreira@ufla.br (S.C.F.); rbgonzatti@unifei.edu.br (R.B.G.)

Abstract: This paper presents a novel strategy for online parameter estimation in a hybrid active power filter (HAPF). This HAPF makes use of existing capacitor banks which it combines with an active power filter (APF) in order to dynamically compensate reactive power. The equipment is controlled with finite control set model predictive control (FCS-MPC) due to its already well-known fast dynamic response. The HAPF model is similar to a grid-connected LCL-filtered converter, so the direct control of the HAPF current can cause resonances and instabilities. To solve this, indirect control, using the capacitor voltage and the inverter-side current, is applied in the cost function, which creates high dependency between the system parameters and the equipment capability to compensate the load reactive power. This dependency is evaluated by simulations, in which the capacitor bank reactance is shown to be the most sensitive parameter, and, thus, responsible for inaccuracies in the FCS-MPC references. In order to minimize this problem without increasing the complexity of the FCS-MPC algorithm, an estimation technique, based on adaptive notch filters, is proposed. The proposed algorithm is tested in a laboratory prototype to demonstrate its ability to follow variations in the HAPF capacitor reactance, effectively correcting the reactive power reference and providing dynamic reactive power compensation. During the tests, the proposed algorithm was capable of keeping the supplied reactive power within a 1% error, even in a situation with 33% variation in the HAPF capacitor reactance.

Keywords: dynamic reactive power compensation; finite control set model predictive control; hybrid active power filter; LCL-filter; model predictive control; parameter estimation

1. Introduction

Hybrid active power filters (HAPFs) are a widely discussed type of equipment used for reactive and harmonic compensation [1,2]. When an active power filter (APF) is connected in series with a shunt passive filter it is possible to reduce the APF rating and improve the passive filter tuning, since the APF is able to electronically change the passive filter impedance. In [3], the concept of active impedance is extended and the passive filter replaced by a capacitor bank. The APF is controlled as a smart impedance to compensate reactive power and harmonics. This HAPF topology is a reliable and cost-effective solution as it eliminates the need for an inductor and can be applied to an existing and operational capacitor bank.

This particular HAPF has been studied for power quality improvement of a single phase low voltage microgrid [4], for reactive power compensation [5] and to compensate both harmonic and reactive power using a multilevel converter topology [6]. The reactive power compensation strategies require a fast response from the equipment in order to properly compensate for dynamic loads, such as in welding, arc furnaces, and wind

generation, among others. In [5,6], this requirement is fulfilled by controlling the HAPF with finite control set model predictive control (FCS-MPC).

In fact, the application of FCS-MPC for power electronics converters has been studied for several years, due, specifically, to its fast dynamic response and its ability to consider systems' nonlinearities and constraints [7]. However, the FCS-MPC depends on the model parameters to select the control action applied to the system. Thus, parameter mismatches have an effect on the prediction of the state variables. This can result in inadequate cost function evaluation and, consequently, incorrect determination of the switching state. Which, in turn, may increase the THD and the steady-state error or even lead to instability in the system.

Due to the FCS-MPC nonlinear characteristic, it is not trivial to evaluate the effects of parameter uncertainties. The most common way to evaluate the system behavior against parameter mismatch is empirical, by analyzing the effects of these variations in the controlled current throughout several scenarios. In [8], the authors take a mathematical approach to evaluating the prediction errors on an L-Filtered converter and conclude that variations in the series resistance are related to steady-state errors, while inductance mismatches cause an increase in the output current ripple, which is responsible for a higher THD. An expansion of this same analysis was produced in [9,10]. In these studies, the authors also considered the errors related to the model discretization and the sampling. Furthermore, a compensation method was formulated and tested in a laboratory setup.

Recently, solutions for parameter mismatch based on model-free predictive control approaches have also been investigated for L-filtered converters [11–13]. In [11] a neural predictor is integrated with a data-driven technique to predict unknown nonlinear system dynamics, model variations, and environment changes. In [12], the proposal was to eliminate the system model using a first-order auto-regressive model with exogenous input (ARX), and the parameters were estimated using a recursive least square (RLS) algorithm. Following this, in [13] the RLS algorithm is improved by using a dynamic-forgetting factor-based bias. Both techniques present a robust response to parameter mismatch. However, all proposals require a deep change in the control algorithm structure.

On the other hand, when FCS-MPC is applied to control an LCL-Filtered converter, which is the case for the HAPF topology used in this work, the method is prone to instabilities due to the delay in the model caused by the capacitor. Furthermore, the presence of the capacitor influences the FCS-MPC capacity to anticipate resonances. According to [14], these instabilities can be avoided without increasing the prediction horizon by defining a proper cost function. In such a case, the cost function can indirectly control the grid-side current by controlling the inverter-side current, or by simultaneously controlling the inverter-side current and capacitor voltage. These references are calculated from the grid-side current reference and the mathematical model of the system. As a consequence, besides the errors in the predicted state variables (model uncertainties), the inaccuracies in parameters can also influence the calculation of the control references, which results in considerable deviations in the equipment's operating point.

Due to the increase in the complexity of FCS-MPC in LCL-Filtered converters, research into parameter estimation techniques is quite recent and a wide range of investigation is still lacking. To the best of the authors' knowledge, the main papers that address these methods can be categorized, according to the purpose of the estimation algorithm, into the following: estimation algorithms to correct the FCS-MPC model uncertainties [15–17] and estimation algorithms to correct FCS-MPC control references uncertainties [18].

Regarding the correction of uncertainties in the model, in [15] the authors propose an adaptive gradient descent optimization method to fulfil this requirement. The results have higher accuracy and faster dynamic response when compared to a traditional state-feedback parameter identification method. A similar proposal is evaluated in [16], but the authors utilize a moth–flame-optimization method. Finally, a model-free predictive control is proposed in [17]. In this paper, the concept of [12] is extended, and the RLS estimation algorithm is used to fit the parameters of a high order ARX model. However, in all of these

papers a significant change in the FCS-MPC original structure is required, increasing the complexity of the control algorithms.

In contrast, the correction of uncertainties in the control references is addressed in [18]. The authors utilize a grid voltage observer and a Luenberger observer to estimate the grid voltage, the capacitor voltage, the inverter-side current and the grid-side current. The grid voltage observer is used to generate the reference of the grid-side current, which is used in the FCS-MPC cost function. The proposal eliminates the need for several sensors and only the grid-side current is measured. The results show satisfactory performance for both steady state and dynamic response.

To summarize, the revised papers solve the problem of parameter uncertainties with estimation methods (such as state observers), or by modifying the structure of the FCS-MPC (such as model-free predictive proposals). They focus on L-filtered converters or LCL-filtered grid-connected converters. This paper, on the other hand, aimed to investigate parameter uncertainties of a Hybrid Active Power Filter, and to solve this problem so as to increase the robustness of this particular equipment, providing accurate reactive power compensation even with variations in the HAPF passive elements. Although the HAPF has the same mathematical model for the FCS-MPC prediction stage, its topology is different. The active part of the equipment is not connected to the point of common coupling (PCC). Thus, the output voltage of the LCL-Filter fluctuates between the grid voltage and the capacitor bank voltage. As a consequence, the equations for the control references calculation are strongly dependent on the capacitor bank reactance [5].

In order to solve the problems related to parameter uncertainties in the control references calculation, this paper proposes a new method to estimate the capacitor bank reactance in the HAPF. The main contributions of this study include the following:
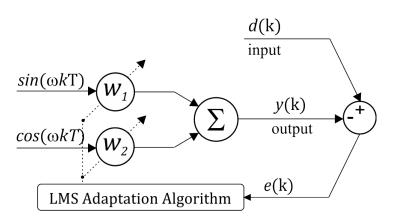
1. The use of the weights of an adaptive notch filter (ANF) and the mathematical model of the system to estimate the capacitor bank reactance;
2. No extra estimator is needed, since these ANFs are already used by the control algorithm to take the state variables to the *dq* coordinate system, as a substitute for the synchronous reference frame (SRF);
3. The online estimation provides a way for the equipment to keep its operation in the case of a fault in a capacitive cell from the equipment's capacitor bank.

As previously discussed, the analysis of the parameter uncertainties on the FCS-MPC prediction stage are not be considered here. In addition, the cost-function definition and the FCS-MPC control itself have been already discussed in [5]. The focus of this paper is the application of the proposed online estimation technique to avoid deviations in the equipment operating point related to ill-calculated references. The method is implemented in a 7.5-kVA single-phase HAPF prototype in order to prove the effectiveness of the algorithm.

This paper is organized as follows: Section 2 explains the ANF structure used to obtain the control references and the parameter estimates; the HAPF topology and the main control strategy are both presented in Section 3; Section 4 describes the proposed method of parameter estimation; the results obtained in a laboratory setup are presented in Section 5 and 6 provides the conclusions.

2. Adaptive Notch Filter

The ANF structure, presented in Figure 1, was first introduced in [19] for noise canceling, but, due to its characteristics, it has been applied for several different purposes in the field of electrical engineering, such as reactive power and harmonics detection and compensation [20] and power calculations [21], among others. The main advantages of this ANF are the easy bandwidth control and adaptive tracking of the fundamental frequency component of the signal.

Figure 1. Adaptive Notch Filter Structure Used for Reactive Power Extraction, Control References Calculation and Parameter Estimation.

The input signal ($d(k)$) is assumed to be any kind of signal, or combination of signals, corrupted by noise. The input references are a pure sine and cosine wave with fundamental frequency ω. The output signal ($y(k)$) is a linear combination of the reference signals and the adaptive weights (w_1 and w_2). The error ($e(k)$) is used in the Least Mean Square (LMS) algorithm for adaptation. The operation of the LMS algorithm for updating the weights is given by:

$$w_1(k+1) = w_1(k) + \mu e(k) \sin(\omega kT) \tag{1}$$

$$w_2(k+1) = w_2(k) + \mu e(k) \cos(\omega kT) \tag{2}$$

where, μ is the step-size value and determines the bandwidth ($BW = 2\mu/T$) and the convergence rate of the algorithm and T is the sampling period. For this structure, it is possible to assure stability for all values of the step size in the range of $0 < \mu < 0.5$ [19].

This ANF has only two coefficients. Therefore, its computational complexity is relatively small when compared to other structures [22]. When applied to the extraction of electrical signal characteristics, such as voltage and current, the sine and cosine are provided by a PLL synchronized with a reference voltage. In this study, all ANFs were synchronized with the source voltage. Thus, the objective of filtering was to guarantee that $y(k)$ tracks the amplitude and phase of the component with frequency ω from the signal $d(k)$. As a consequence, the weights w_1 and w_2 carry relevant information about the fundamental component.

So, assuming the output signal is a pure sine wave, with amplitude A, phase ϕ, and frequency ω, it is represented as:

$$y(k) = A \sin(\omega kT + \phi) \tag{3}$$

Using the trigonometric identities, we can also represent (3) as:

$$y(k) = A \cos(\phi) \sin(\omega kT) + A \sin(\phi) \cos(\omega kT) \tag{4}$$

On the other hand, as shown in Figure 1, the ANF output signal is given by:

$$y(k) = w_1(k) \sin(\omega kT) + w_2(k) \cos(\omega kT) \tag{5}$$

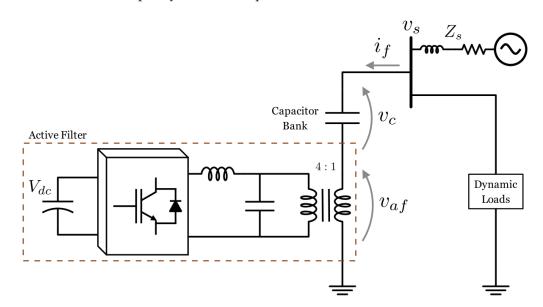Comparing (4) and (5), we obtain:

$$w_1(k) = A \cos(\phi) \tag{6}$$

$$w_2(k) = A \sin(\phi) \tag{7}$$

An analogy can be made between the ANF weights and the SRF direct and quadrature components (*dq* components). However, the ANF has better dynamic response and a shorter processing time than the SRF, as explained in [21].

In this paper, the presented ANF structure is used to extract the load reactive current component, which is applied to calculate the control references for reactive power compensation. The main contribution of this study is also the use of this same ANF structure to estimate the HAPF parameters by means of the ANF weights and the system mathematical model.

3. Hybrid Active Power Filter Control with FCS-MPC

The operating principle of the HAPF topology used in this work was extensively discussed in [3]. In spite of the equipment's capability to compensate for reactive power and harmonic frequencies, in this work only the reactive power control loop is explored. This equipment can be applied to compensate the reactive power of dynamic loads, such as arc furnaces, wind farms, fluctuating reactive loads, and welding operations, among others. The simplified diagram of the HAPF is shown in Figure 2, where v_{af}, v_c, v_s and V_{dc} are the active filter voltage, the capacitor bank voltage, the source voltage and the DC link voltage, respectively and i_f is the hybrid filter branch current, which is predominantly capacitive at the fundamental frequency due to the capacitor bank.

Figure 2. Hybrid Active Power Filter Topology Composed by an Active Filter and a Capacitor Bank Used for Reactive Power Compensation.

Proper control of the filter current (i_f) assures dynamic compensation of reactive power. In this HAPF topology, the control of i_f is performed by applying the necessary voltage to v_{af}, which, in turn, controls the voltage over the capacitor bank so that the reactive component of i_f follows a given reference.

In [5] the use of FCS-MPC was proposed to improve the HAPF transient response, as an alternative to classical controllers in the SRF. The FCS-MPC aims to minimize a cost function by evaluating the discrete model of the system only for the finite-set of possible switching states of the converter [23]. The main aspects for successful implementation of FCS-MPC are proper system modeling and cost function definition, which are summarized in the next sections.

3.1. HAPF Modeling

In order to model the HAPF, its variables were considered in per-unit (pu) values and the transformer was modeled by means of its series impedance, as detailed in [5]. As a result, the complete circuit of the HAPF is presented in Figure 3.
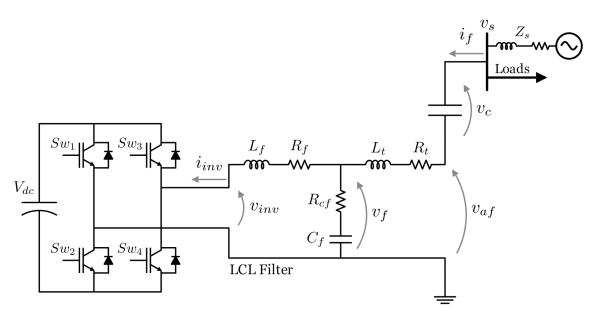
Figure 3. Complete Hybrid Active Power Filter Equivalent Circuit.

Note the following: L_f and R_f are the inverter filter inductance and its inner resistance; C_f and R_{cf} are the filter parallel capacitance and its inner resistance; R_t and L_t are the short circuit transformer resistance and inductance, respectively. In addition, v_{inv} and i_{inv} are the inverter voltage and current, v_f is the filter capacitor voltage and Sw_n are the switching devices. Due to the coupling transformer, the *pu* representation makes state–space modeling easier. The state–space model of the HAPF is described in [5]:

$$\dot{x}(t) = \mathbf{A}x(t) + \mathbf{B}u(t) \tag{8}$$

$$\frac{d}{dt}\begin{bmatrix} i_{inv} \\ i_f \\ v_f \end{bmatrix} = \mathbf{A}\begin{bmatrix} i_{inv} \\ i_f \\ v_f \end{bmatrix} + \mathbf{B}\begin{bmatrix} v_{inv} \\ v_{af} \end{bmatrix} \tag{9}$$

where,

$$\mathbf{A} = \begin{bmatrix} -\dfrac{R_f}{L_f} & 0 & \dfrac{1}{L_f} \\ 0 & -\dfrac{R_t}{L_t} & -\dfrac{1}{L_t} \\ \left(\dfrac{R_f \cdot R_{cf}}{L_f} - \dfrac{1}{C_f}\right) & \left(\dfrac{1}{C_f} - \dfrac{R_t \cdot R_{cf}}{L_t}\right) & -R_{cf} \cdot \left(\dfrac{1}{L_f} + \dfrac{1}{L_t}\right) \end{bmatrix} ; \mathbf{B} = \begin{bmatrix} -\dfrac{1}{L_f} & 0 \\ 0 & \dfrac{1}{L_t} \\ \dfrac{R_{cf}}{L_f} & \dfrac{R_{cf}}{L_t} \end{bmatrix} \tag{10}$$

The discretization of the state–space model from (9) is written as:

$$\begin{bmatrix} i_{inv}(k+1) \\ i_f(k+1) \\ v_f(k+1) \end{bmatrix} = \mathbf{A}_d\begin{bmatrix} i_{inv}(k) \\ i_f(k) \\ v_f(k) \end{bmatrix} + \mathbf{B}_d\begin{bmatrix} v_{inv}(k) \\ v_{af}(k) \end{bmatrix} \tag{11}$$

Where, k is the sampling instant and $\mathbf{A}_d$ and $\mathbf{B}_d$ are the discrete forms of the matrices $\mathbf{A}$ and $\mathbf{B}$ shown in (10). The system model discretization is realized by the forward Euler method and, since a high sampling frequency is used (40 kHz), it is possible to ignore higher order terms, which results in [14]:

$$\mathbf{A}_d = \exp^{\mathbf{A}T_s} \approx I + \mathbf{A}T_s \tag{12}$$

$$\mathbf{B}_d \approx \mathbf{B}T_s \tag{13}$$

where T_s is the sampling period. The discrete HAPF model is used to predict the state variables for the next sampling instants. In this work, a single-phase H-Bridge converter was used. However, the concepts can be extended for three-phase and multilevel converters, as in [6]. For single-phase inverters, the algorithm must consider four switching states (S_n), which results in the following voltage vectors: $v^0 = 0$, $v^1 = V_{dc}$, $v^2 = -V_{dc}$ and $v^3 = 0$.

3.2. Cost Function Definition

In LCL-Filtered converters, the direct control of i_f is not trivial and usually requires longer prediction horizons ($N > 2$). The filter capacitor introduces a delay in the model equations, and, thus, the manipulated variable (v_{inv}) is no longer related to the controlled variable (i_f) in the next sampling instant, as in L-Filter models [24]. Aiming to avoid long prediction horizons and the consequent increase in processing time, the application of FCS-MPC with a multi-variable cost function was presented in [14,25]. According to this study, the application of a multi-variable cost function to control more than one of the LCL-Filter state variables is a simple way to assure stability and avoid resonances. So, here, the control of the inverter output current (i_{inv}) guarantees the system's stability, while the filter capacitor voltage (v_f) control is responsible for avoiding harmonics and resonances. As a result, the multi-variable cost function is given by:

$$J = \lambda_i |i_{inv}^* - i_{inv}^P|^2 + \lambda_v |V_{f_{AD}}^* - v_f^P|^2 \tag{14}$$

where λ_i and λ_v are the cost function gains which define the control priorities, i_{inv}^* and i_{inv}^P are the reference and the predicted values of the inverter output current, $V_{f_{AD}}^*$ is the filter capacitor voltage reference, considering the resonance active damping, as shown in Section 3.4 and v_f^P is the predicted value of the filter capacitor voltage, respectively. A prediction horizon of $N = 2$ was adopted. First, the state variables are estimated for the next sampling instant in order to compensate for the delay caused by the processing time, and, then, the cost function is evaluated for the predicted state variables two instants ahead [26].

In a typical FCS-MPC application the cost function may also contain other terms that are designed to consider system nonlinearities, constraints or other secondary control objectives. Examples of these include the following: reduce common-mode voltages [27], apply converter output current limitations [28,29], reduce thermal stress on semiconductor devices [30], reduce losses by penalizing the number of semiconductor commutations [15,31], and control the converter switching frequency [32], among others. However, since the objective of this paper was to demonstrate the effectiveness of the proposed parameter estimation technique, the cost function was kept as simple as possible and no constraints were considered.

3.3. Control References

The FCS-MPC with multi-variable cost function deals with the drawbacks of LCL-Filtered converter control. Nonetheless, since the control is based on the hybrid filter current reference (i_f^*), the control references for the capacitor filter voltage (v_f^*) and for the inverter current (i_{inv}^*) must be obtained indirectly by the system model. In the following sections, a summary of the control references calculation is presented, and the detailed equations are presented in [5].

3.3.1. Reference of Hybrid Filter Current (i_f^*)

The reference current i_f^* controls the reactive power delivered by the HAPF and assures DC link voltage regulation. This current can be represented using the *dq* axes:

$$i_f^* = I_f^{d*} \sin(\omega kT) + I_f^{q*} \cos(\omega kT) \tag{15}$$

The active current is controlled by the direct axis component (I_f^{d*}), which is responsible for the DC link voltage regulation and is obtained by a PI controller. The reactive current is controlled by the quadrature component of the current (I_f^{q*}), which is responsible for the reactive power control. The reactive current reference can be set manually for static operation of the equipment or, in the case of dynamic compensation of load reactive power, this reference is obtained through an ANF applied to the load current (i_L), which results in:

$$i_{L_{ANF}} = w_1^{i_L} \sin(\omega kT) + w_2^{i_L} \cos(\omega kT) \tag{16}$$

where, $i_{L_{ANF}}$ is the output of the ANF, and $w_1^{i_L}$, $w_2^{i_L}$ are its adaptive weights. Considering the result obtained in (7), and the analogy to the SRF, the weight $w_2^{i_L}$ is the quadrature, or reactive component, of the load current. Thus, the hybrid filter reactive current is controlled in such a way that $I_f^{q*} = -w_2^{i_L}$, ensuring the unit power factor in the source.

3.3.2. References of Filter Capacitor Voltage (v_f^*) and Inverter Output Current (i_{inv}^*)

As previously discussed, the state variables that are actually controlled are the filter capacitor voltage (v_f) and the inverter output current (i_{inv}). The references for these variables are based on the HAPF current reference (i_f^*) and the system model. The system model is derived from the equivalent circuit, shown in Figure 3. Using a phasor representation, the reference variables are calculated as:

$$\begin{bmatrix} \dot{V}_f^* \\ \dot{I}_{inv}^* \end{bmatrix} = \begin{bmatrix} \dot{V}_s \\ 0 \end{bmatrix} + \begin{bmatrix} -(R+jX) & 0 \\ 1 & \left(\dfrac{1}{jX_{cf}}\right) \end{bmatrix} \begin{bmatrix} \dot{I}_f^* \\ \dot{V}_f^* \end{bmatrix} \tag{17}$$

where R is the hybrid filter branch resistance-composed by the capacitor bank series resistance (R_c) and the transformer resistance (R_t) $-$ X is the equivalent reactance of the hybrid filter branch-composed by the inductive reactance of the transformer (X_t) and the capacitive reactance of the capacitor bank (X_c)$-$ and X_{cf} is the filter capacitor reactance. The filter capacitor series resistance is disregarded for the reference calculation. To proceed with the calculations it is assumed that:

$$\dot{I}_f^* = I_f^{d*} + jI_f^{q*} = I_f^{d*} - j(w_2^{i_L}) \tag{18}$$

$$\dot{V}_s = V_s^d + jV_s^q = w_1^{v_s} + j(w_2^{v_s}) \tag{19}$$

As previously stated, the value of I_f^{d*} is obtained through a PI controller and $w_2^{i_L}$ is the coefficient from the ANF applied to the load current. Then, another ANF is applied to the source voltage, which provides the coefficients $w_1^{v_s}$ and $w_2^{v_s}$ used in the phasor representation of this variable. In addition, $\dot{V}_f^*$ and $\dot{I}_{inv}^*$ can also be represented as:

$$\dot{V}_f^* = V_f^{d*} + jV_f^{q*} \tag{20}$$

$$\dot{I}_{inv}^* = I_{inv}^{d*} + jI_{inv}^{q*} \tag{21}$$

where, V_f^{d*} and I_{inv}^{d*} are the direct components of the capacitor voltage and inverter current references, and V_f^{q*} and I_{inv}^{q*} are the quadrature components of the capacitor voltage and inverter current references, respectively. Finally, the time domain references, v_f^* and i_{inv}^*, are obtained as:

$$v_f^* = V_f^{d*} \sin(\omega kT) + V_f^{q*} \cos(\omega kT) \tag{22}$$

$$i_{inv}^* = i_{inv}^{d*} \sin(\omega kT) + i_{inv}^{q*} \cos(\omega kT) \tag{23}$$

It is noteworthy that this method uses the system model and one extra ANF to calculate the references for v_f and i_{inv}. The overall control processing time is not significantly increased, and the need for long prediction horizons is avoided. In fact, in [5,14] the authors already demonstrated the effectiveness of using FCS-MPC with a multivariable cost function and estimated references. However, they highlighted that model inaccuracies could make this approach prone to current deviations from the set point. This can be realized by analyzing (17), since the parameter values are directly related to the references being calculated, deviations in these values are translated into incorrect references, which are tracked by the FCS-MPC and cause the equipment to operate outside the desired point.

3.4. Resonance Damping Method

In order to dampen the resonances, and to block the circulation of harmonic currents due to source voltage distortion, a virtual resistance (R_v) is added to the system. The concept of virtual resistance in series with the output inductance for that purpose is not new [33], having been adopted by several papers with FCS-MPC and other control algorithms [14,24]. To achieve such an effect, the hybrid filter branch current (i_f) is filtered by an ANF to eliminate its fundamental component, the same ANF structure from Figure 1 is applied, and the hybrid filter harmonic content (i_{f_h}) is the error signal obtained. Then, i_{f_h} is multiplied by a virtual resistance (R_v) to generate a damping term to be added to the filter capacitor voltage in order to generate a new reference, as:

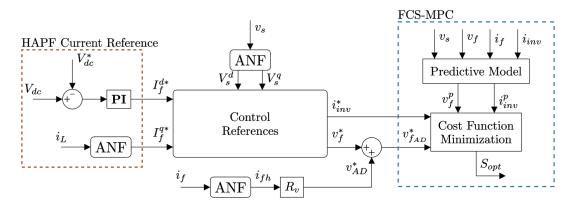$$v_{f_{AD}}^* = v_f^* + R_v i_{f_h} = v_f^* + v_{AD}^* \tag{24}$$

where v_{AD}^* is the active term responsible for the source voltage harmonic damping.

3.5. Summary of FCS-MPC Control Loop

The block diagram of Figure 4 summarizes the control strategy applied to the HAPF. The algorithm is divided into the following blocks: definition of the HAPF branch current reference (i_f^*); FCS-MPC references calculation ($v_{f_{AD}}^*$ and i_{inv}^*); FCS-MPC control loop.

The control references are obtained according to the method described in Section 3.3, and the FCS-MPC control loop follows the steps below:

1. Estimate the system states for $(k+1)$ from (9), in order to compensate for the computation time delay;
2. Predict the system states for $(k+2)$, considering all possible switching states;
3. Evaluate the cost function based on the predicted variables and reference variables previously obtained;
4. Define the optimum switching state (S_{opt}) that minimizes the cost function, which is applied in the next sampling period.

Figure 4. Block Diagram of the Control Strategy Applied to the HAPF without the Proposed Parameter Estimation Method.

In the following section, the influence of parameter mismatch on the control references calculation is discussed and a method to estimate the capacitor bank reactance is proposed.

4. Proposed Method of Parameter Estimation with Adaptive Filters

As previously mentioned, the indirect calculation of the cost function references can result in hybrid filter current (i_f) inaccuracies. This happens because the calculation of v_f^* and i_{inv}^* are directly dependent on the HAPF model parameters, such as the capacitor bank and the transformer reactance. If there is a significant mismatch in those values, or if they vary during the compensation process or over time, the cost function references can be wrongly obtained. As a result, the HAPF ability to properly compensate the load reactive power is affected. It is important to highlight that the proposed method aims to avoid errors caused by deviations in the calculated control references, and the parameter mismatch effects on the FCS-MPC stability and dynamic response are not discussed.

4.1. Evaluation of Parameter Mismatch by Simulations

The FCS-MPC scheme presented in Figure 4 was simulated in order to evaluate which parameter most influences the hybrid filter branch current. Table 1 presents the system setup used for the simulations. The definitions of the control parameters, λ_{inv}, λ_v, R_v, k_p, k_i and μ, are based on [5].
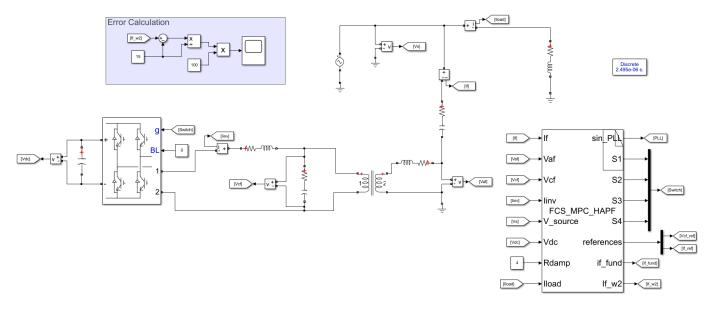
Table 1. System Setup.

System Parameters	
LCL Filter	$L_f = 5.84$ mH; $R_f = 0.2\,\Omega$ $C_f = 11.4\,\mu$F; $R_{cf} = 0.75\,\Omega$ $L_t = 1.06$ mH; $R_t = 0.17\,\Omega$
Transformer	$S = 7.5$ kVA, (440:127 V)
Capacitor Bank	$C = 274\,\mu$F; $R_c = 0.7\,\Omega$
DC Link	$V_{dc} = 400$ V; $C_{dc} = 9000\,\mu$F
Voltage Source	127 V/60 Hz (phase to ground)
DC Link PI Gains	$k_p = 0.1$; $k_i = 0.4$
ANF	$\mu = 0.0055$
FCS-MPC	$\lambda_{inv} = 1$; $\lambda_v = 80$
Sampling Frequency	$f_s = 40{,}080$ Hz

According to (17), the calculation of the reference voltage v_f^* depends on the hybrid filter branch equivalent resistance ($R = R_t + R_c$) and reactance ($X = X_t - X_c$). To measure how each of these parameters affects the hybrid filter response, they were varied in a range of 0.1 to 2 times its real values, and then the hybrid filter branch current deviation from its reference was calculated by:
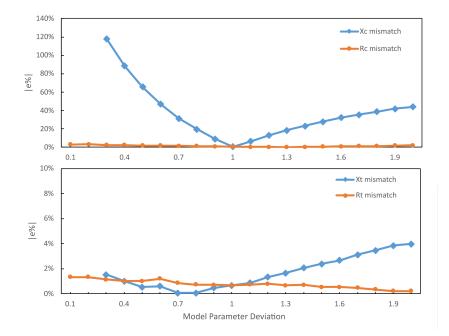
$$e(\%) = \frac{\dot{I}_f - \dot{I}_f^*}{\dot{I}_f^*} \tag{25}$$

Figure 5 depicts the simulation circuit used to study how the variation of each parameter affects the HAPF response. The simulated circuit is the same as the one shown in Figure 2. The simulation results were obtained from several simulations. The first step was to simulate the system with its nominal parameter values, shown in Table 1, and then other simulations, that considered variations in each parameter, were realized and the current deviation was calculated using (25). In all the simulations, a fixed 15 A current reference was considered for I_f^q, and the FCS-MPC algorithm was written in C. The simulations were performed offline, so no complexity was added to the overall FCS-MPC algorithm.

Figure 5. Simulation Circuit Used to Measure the Effect of Parameter Mismatch in the Control Response.

The simulation results for the errors in the magnitude of the hybrid filter current are presented in Figure 6. Both the transformer and the capacitor bank resistances show almost no influence in the control response. The transformer resistance caused amplitude errors smaller than 1.5% and the capacitor bank resistance worst case scenario caused a deviation of 3% in the amplitude of the hybrid filter current. Similarly, the transformer's inductive reactance mismatch results in amplitude errors of up to 4% in the hybrid filter current, although when its value was 3 times lower than its nominal value, the system became unstable. The capacitor bank reactance, on the other hand, significantly influenced the hybrid filter current, resulting in a maximum error of 120% when the model value reached 0.3 times the real one. Parameter deviations smaller than 0.3 and larger than 1.9 took the equipment out of its nominal operation range, reaching the transformer maximum voltage.

Figure 6. Simulation Results Showing the i_f Magnitude Error Due to Model Parameter Mismatch.

It may be concluded that the indirect method for cost function references calculation presents a substantial sensibility to capacitive reactance mismatches when applied to this HAPF topology, since even small variations in its value create great error in the supplied reactive power. In addition, both the capacitor and the transformer reactances can make the system unstable if a large enough variation occurs.

4.2. Parameter Estimation Focused on HAPF Reactance

The proposed method for parameter estimation is based on the application of the ANF structure presented in Section 2. This structure is applied to the source voltage (v_s), the filter capacitor voltage (v_f), the active filter output voltage (v_{af}) and the hybrid filter branch current (i_f), which gives:

$$V_s^d = w_1^{v_s} \; ; \; V_s^q = w_2^{v_s} \tag{26}$$

$$V_f^d = w_1^{v_f} \; ; \; V_f^q = w_2^{v_f} \tag{27}$$

$$V_{af}^d = w_1^{v_{af}} \; ; \; V_{af}^q = w_2^{v_{af}} \tag{28}$$

$$I_f^d = w_1^{i_f} \; ; \; I_f^q = w_2^{i_f} \tag{29}$$

The ANFs applied to v_s and i_f were already needed to perform the control reference calculations, so it was necessary to add the ANFs only to v_f and v_{af}. From the circuit shown in Figure 3, the following formulations in the *dq* reference frame are obtained:

$$\begin{cases} V_s^{dq} - V_{af}^{dq} = (\widehat{R}_c - j\widehat{X}_c)I_f^{dq} \\ V_{af}^{dq} - V_f^{dq} = (\widehat{R}_t + j\widehat{X}_t)I_f^{dq} \end{cases} \tag{30}$$

where, $\widehat{R}_c$ and $\widehat{X}_c$ are the estimated capacitor resistance and reactance, and $\widehat{R}_t$ and $\widehat{X}_t$ are the estimated transformer resistance and reactance. After some mathematical manipulations, the equations in (30) can be written as:

$$\begin{bmatrix} (V_s^d - V_{af}^d) \\ (V_s^q - V_{af}^q) \\ (V_{af}^d - V_f^d) \\ (V_{af}^q - V_f^q) \end{bmatrix} = \begin{bmatrix} I_f^d & I_f^q & 0 & 0 \\ I_f^q & -I_f^d & 0 & 0 \\ 0 & 0 & I_f^d & -I_f^q \\ 0 & 0 & I_f^q & I_f^d \end{bmatrix} \begin{bmatrix} \widehat{R}_c \\ \widehat{X}_c \\ \widehat{R}_t \\ \widehat{X}_t \end{bmatrix} \tag{31}$$

Rewriting these equations and substituting the relations shown in (26) through (29) we obtain:

$$\widehat{R}_c = \frac{(w_1^{v_s} - w_1^{v_{af}})(w_1^{i_f}) + (w_2^{v_s} - w_2^{v_{af}})(w_2^{i_f})}{(w_1^{i_f})^2 + (w_2^{i_f})^2} \tag{32}$$

$$\widehat{X}_c = \frac{(w_1^{v_s} - w_1^{v_{af}})(w_2^{i_f}) - (w_2^{v_s} - w_2^{v_{af}})(w_1^{i_f})}{(w_1^{i_f})^2 + (w_2^{i_f})^2} \tag{33}$$

$$\widehat{R}_t = \frac{(w_1^{v_{af}} - w_1^{v_f})(w_1^{i_f}) + (w_2^{v_{af}} - w_2^{v_f})(w_2^{i_f})}{(w_1^{i_f})^2 + (w_2^{i_f})^2} \tag{34}$$

$$\widehat{X}_t = \frac{-(w_1^{v_{af}} - w_1^{v_f})(w_2^{i_f}) + (w_2^{v_{af}} - w_2^{v_f})(w_1^{i_f})}{(w_1^{i_f})^2 + (w_2^{i_f})^2} \tag{35}$$

which are the formulations implemented in the algorithm for the online estimation of the hybrid filter branch parameters. Once these parameters are calculated, it is possi-

ble to obtain the estimated value for the total hybrid filter branch resistance ($\widehat{R}$) and reactance ($\widehat{X}$) through:

$$\begin{cases} \widehat{R} = \widehat{R}_t + \widehat{R}_c \\ \widehat{X} = \widehat{X}_t - \widehat{X}_c \end{cases} \tag{36}$$

By using the values estimated in (17), the control references are modified and the HAPF operating point is corrected. It is also possible to use the estimated values to obtain an estimation of the real values of the capacitor bank capacitance and the transformer inductance through:
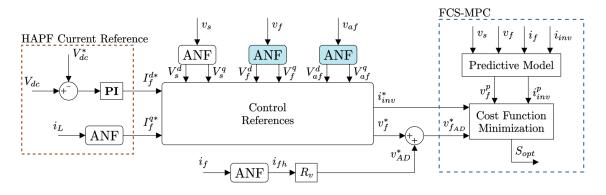
$$\widehat{C} = \frac{1}{\omega \widehat{X}_c} \tag{37}$$

$$\widehat{L}_t = \frac{\widehat{X}_t}{\omega} \tag{38}$$

where ω is the grid angular frequency, $\widehat{C}$ is the estimated value of the capacitor bank capacitance and $\widehat{L}_t$ is the estimated value of the transformer inductance.

Singular importance is given to $\widehat{C}$, since its value may be used to keep track of faults in a capacitive cell or even adjust the equipment operating point online, depending on the load reactive power, thereby effectively increasing the equipment operating range.

As previously discussed, the application of the proposed method only requires two more ANFs to be added to the system. The new block diagram with the proposed parameter estimation method is shown in Figure 7 in which the blue blocks represent the ANFs that were introduced to the system.
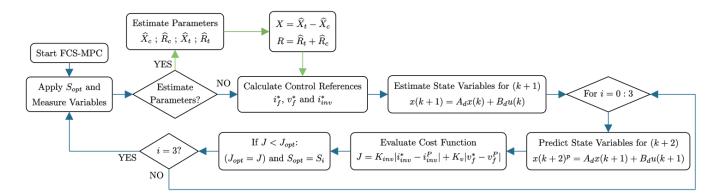

Figure 7. Block Diagram of the Control Strategy Applied to the HAPF with the Proposed Parameter Estimation Method.

4.3. Implementation Aspects of the Proposed FCS-MPC with Parameter Estimation

The flowchart of Figure 8 shows the implementation of the FCS-MPC algorithm with the proposed method for parameter estimation. According to the flowchart, in every sampling period, the FCS-MPC algorithm begins by applying the S_{opt} defined in the last sampling period and measuring the system variables, namely v_s, v_f, v_{af}, i_{inv}, i_f and i_L. Then, if the online estimation is active, the algorithm estimates the system parameters by means of Equations (32) through (35), which are used to calculate the control references. If the online estimation algorithm is not active, the references are calculated using the predefined impedance values.

The state variable measurements and the control output being currently applied to the system ($V_{inv}(k)$) are used to estimate the state variables for the next sampling period ($k+1$). The estimated values are applied to the system model to predict the values for the instant ($k+2$) considering every possible converter switching state. Finally, the predicted values are evaluated by the cost function and the optimum switching state is selected to be applied in the next sampling period.

Figure 8. Flowchart of the Proposed FCS-MPC Strategy with Control Reference Adjustment Based on Parameter Estimation.

5. Results

The proposed method for parameters estimation was tested in a laboratory setup assembled according to the diagram shown in Figure 2. The system setup followed the one described in Table 1 for the simulations and the hardware used to run the algorithm was a DSP TMS320F28379D. The HAPF laboratory setup is shown in Figure 9.

In order to properly evaluate the algorithm response to variations in the capacitor bank reactance value, the setup was composed of 4 paralleled capacitors, one of which was connected through a contactor, which allowed the capacitor bank value to be changed during the equipment's operation, simulating a fault in one of the capacitors. Each capacitor had a nominal value of 68.5 µF, which made for a total of 274 µF when all capacitors were connected and 205.5 µF when one of them was removed.

To test the algorithm's response to multiple scenarios, the tests were divided into two: first, a fixed reactive power reference was provided to the FCS-MPC; and, in the second test, the HAPF compensated the reactive power from a load. In both tests the capacitor bank value was changed during the equipment's operation. It is important to note that the capacitor bank value was set to 274 µF during the algorithm's initialization. Therefore, this is the value considered by the reference generation algorithm when the parameter estimation is not activated, regardless of the number of capacitors connected to the capacitor bank.
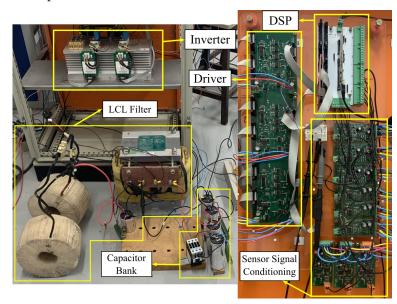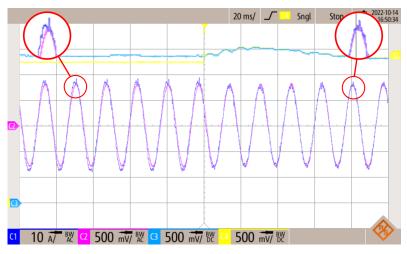

Figure 9. HAPF Laboratory Setup.

5.1. Fixed Reactive Power

To visualize the algorithm's capability to adjust the HAPF branch current to its reference, Figure 10 shows the moment when the estimation algorithm is activated. The peak value for the HAPF reactive current reference (I_f^{q*}) is set to 16 A, the oscilloscope channel 1 (Blue) shows the HAPF current, channel 2 (Pink) shows the current reference, channel 3 (Cyan) is the estimated capacitor bank capacitance and channel 4 (Yellow) is the capacitance value being used in the control reference calculation. A 100 μF/V relation was used to plot the capacitance values from the filtered DSP PWM outputs.
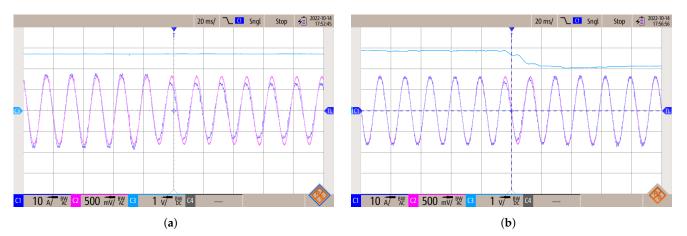
Before the prediction algorithm was activated, the capacitance value used in the control reference calculations was the nominal 274 μF, shown in yellow. However, the real capacitance value estimated by the algorithm was around 286 μF. This created an error between the reference value and the actual HAPF current. Once the estimation algorithm was activated there was a little overshoot in the estimated value, due to the changes in the control references, but, after around 3.5 cycles, the estimated values returned to the correct values. Nevertheless, the HAPF current followed the correct reference as soon as the estimated values began to be used in the reference calculations. After the activation of the estimation algorithm, some perceptible oscillations appeared in the estimated capacitance value. This occurred as a result of the ANF adaptation times, and ceased once the weights were fully adapted.

Figure 10. HAPF Branch Current (C1) and Capacitor Value (C4) Adjustment with the Proposed Estimation Algorithm.

Figure 11 shows the HAPF current behavior when one of the capacitors is removed from the capacitor bank. In this figure, the cyan line indicates the capacitance value used by the control reference calculation. In Figure 11a, the estimation algorithm was not activated, so the capacitance used in the control reference calculation kept its value of 274 μF for the entire time, which created a considerable error between the HAPF current and its reference value. Figure 11b shows the case where the online parameter estimation was activated. After the removal of one capacitor from the capacitor bank, its estimated capacitance changed from 286 μF to 215 μF. This guaranteed that the HAPF kept supplying the desired reference and the capacitance value adjustment was completed in around 1.5 fundamental cycles.

The result of Figure 11b also demonstrates the estimated capacitance value behavior prior, during, and after a big variation in the capacitor bank value. As previously discussed, the oscillations in the estimated capacitance value, when the estimation algorithm was activated, (Figure 10), disappeared when the ANFs' weights were fully adapted. This was demonstrated by the estimated value prior to the capacitor bank variation, in Figure 11b, which had no oscillations. When the capacitor was removed from the capacitor bank some oscillations were visible, due to the adaptation process of the ANFs' weights, but, once again, these oscillations only occurred while the weights were being adapted.

(**a**)   (**b**)

Figure 11. Capacitor Bank Capacitance Considered by the Control Algorithm (C3) and HAPF Branch Current Response (C1) to Variation in the Capacitor Bank Value (**a**) without Online Estimation and (**b**) with Online Estimation.

Another important variable to visualize is the filter capacitor voltage (v_f) when the capacitor bank value changed, which is shown in Figure 12. Now, the oscilloscope channel 1 (Blue) shows the filter capacitor voltage, channel 2 (Pink) shows the filter capacitor voltage reference ($v^*_{f_{AD}}$) and channel 3 (Cyan) still shows the capacitor bank capacitance used in the control reference calculation. As expected, when one capacitor was removed from the capacitor bank its total capacitance reduced, so, in order to keep supplying the same current, as already shown in Figure 11b, the voltage across the capacitor bank had to be increased. This effect was achieved by reducing the voltage over the active part of the HAPF and, likewise, the filter capacitor voltage reference was reduced.
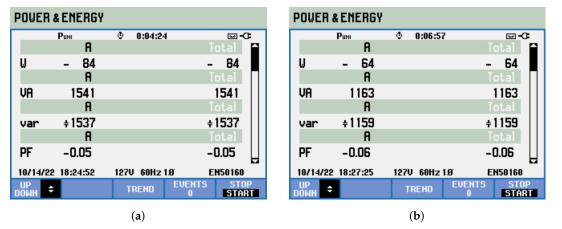

Figure 12. Capacitor Bank Capacitance Considered by the Control Algorithm (3) and Filter Capacitor Voltage Response (C1) to Variation in the Capacitor Bank Value with Online Estimation.

When a fixed reactive current reference was provided to the FCS-MPC algorithm the HAPF acted as a capacitor bank, supplying the desired reactive power. Before the application of the proposed algorithm for parameter estimation, the power supplied by the HAPF was measured for a configuration with four and three capacitors, respectively. In both measurements, the reactive current reference was kept at 16 A. The results are shown in Figure 13.
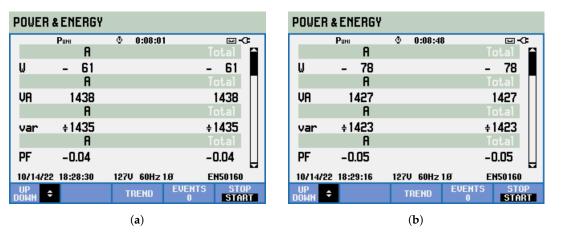
The actual value that the HAPF must supply when $i^{q*}_f = 16$ A should be around 1436 Var, depending on the source voltage level, but, as depicted in Figure 13a, even when the capacitor bank was operating with its nominal value of 274 μF, the reactive power measured was not the correct one, sitting around 1537 Var. This was due to variations in
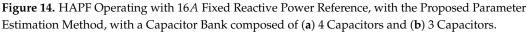
the real value of the capacitors and some source voltage fluctuations. When one capacitor was removed from the capacitor bank, the reactive power value moved even further away from the expected value, as shown in Figure 13b.

(a)

(b)

Figure 13. HAPF Operating with 16*A* Fixed Reactive Power Reference, without the Proposed Parameter Estimation Method, with a Capacitor Bank composed of (**a**) 4 Capacitors and (**b**) 3 Capacitors.
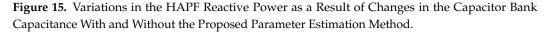
Once the online parameter estimation algorithm was activated, the reactive power supplied moved to a value closer to the expected one, as shown in Figure 14. Figure 14a shows the result for a capacitor bank with 4 capacitors. The equipment supplied 1435 Var, which was a value very close to the nominal. The small variation observed may be the result of a fluctuation in the source voltage value. When one capacitor was removed from the capacitor bank there was almost no change in the HAPF reactive power, as shown in Figure 14b. This demonstrates the effectiveness of the proposed method.

(a)

(b)

Figure 14. HAPF Operating with 16*A* Fixed Reactive Power Reference, with the Proposed Parameter Estimation Method, with a Capacitor Bank composed of (**a**) 4 Capacitors and (**b**) 3 Capacitors.

The comparison between the delivered power of the HAPF when operating with and without the estimation algorithm is shown in Figure 15. In this test, the same 16 A reactive current reference was used. First, the online estimation algorithm was not being used, indicated by the red arrows, and, hence, the delivered power dislocated from its desired value, even for the nominal capacitance value. Once one capacitor was removed, the HAPF delivered power suffered a great change. At the point indicated by 40 s, the online estimation algorithm was activated, indicated by the blue arrows, and the delivered power shifted to the correct value. After a few seconds, the capacitor that was previously removed was once again connected to the capacitor bank, and the delivered power was kept at the reference value. The small variation that occurred at this point was the same as that shown in Figure 14.

Figure 15. Variations in the HAPF Reactive Power as a Result of Changes in the Capacitor Bank Capacitance With and Without the Proposed Parameter Estimation Method.

5.2. Dynamic Reactive Power Compensation

When a HAPF is applied to dynamically compensate the reactive power of loads connected to the system, it is important that the power factor at the point of connection is kept unitary. To test how the equipment's load compensation capability would act under capacitor bank variations, a test load was set, and its power measurement is shown in Figure 16.
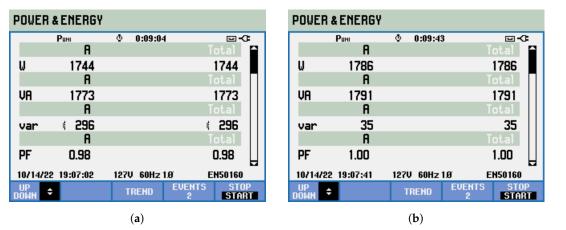

Figure 16. Load Power Measurement.

First, the HAPF compensation was tested with the capacitor bank operating with 4 capacitors, with and without the estimation algorithm. The results are shown in Figure 17. Without the estimation algorithm, a small error was observed at the HAPF point of coupling, as shown in Figure 17a. This overcompensation indicated that the real value of the capacitor bank capacitance was larger than the one considered by the reference generation algorithm, also indicated by the result shown in Figure 10. Once the estimation algorithm was activated, the HAPF compensation corrected and a unit power factor was obtained, as depicted in Figure 17b.

The equipment was then tested with only 3 capacitors connected to the capacitor bank while the same load was being compensated, and the results are shown in Figure 18. When the estimation algorithm was not active, the HAPF was not capable of fully compensating the load's reactive power, as depicted in Figure 18a. This happened because the reference generation algorithm was considering a larger value for the capacitor bank than the one actually connected to the HAPF branch. The result shown in Figure 18b demonstrates that, when the online estimation algorithm was activated, the HAPF was

able to properly compensate the load's reactive power, and guaranteed a unit power factor at the coupling point.

(**a**)   (**b**)

Figure 17. Load Reactive Power Compensation with a 274 µF Capacitor Bank (**a**) without Parameter Estimation and (**b**) with Parameter Estimation.

(**a**)   (**b**)

Figure 18. Load Reactive Power Compensation with a 205.5 µF Capacitor Bank (**a**) without Parameter Estimation and (**b**) with Parameter Estimation.

Finally, regarding the computational burden, the parameters estimation algorithm used four ANFs applied to the system state variables. Each ANF had an execution time of 0.683 µs (running in a TMS320F28379D at 200 MHz), which resulted in a total time of 2.73 µs when all four ANFs were being executed. The ANF structure employed was chosen due to its computational efficiency and ease of implementation. As explained in Section 3, two of the four ANFs were already required by the control reference calculation algorithm, so only two extra ANFs were added, one for v_f and one for v_{af}. The estimation of the system parameters was calculated by Equations (32) through (35), which took around 4 µs to be executed, mainly due to the divisions required by the equations. The total execution time for the control algorithm without the parameter estimation was 14.9 µs (including the PLL and the complete control strategy shown in Figure 4). After the addition of the proposed parameter estimation algorithm, the total execution time increased to 20.3 µs, which enabled a sampling frequency of 40,080 Hz.

6. Conclusions

The FCS-MPC is a control technique known to suffer deviations in its response depending on the accuracy of the model parameters. This problem is even more pronounced when the control references are also obtained from the system model. Considering these problems, this work proposed an algorithm to estimate the system parameters used in the control reference calculation during the equipment's operation. First, a study was con-

ducted to evaluate how each of the parameters' errors influenced the reference calculation, and it was observed that the most significant deviation was due to uncertainties in the HAPF capacitor bank impedance. Thus, the proposed algorithm was built based on the information provided by four ANFs. Only two extra ANFs were applied, since the other two were already required for the control reference calculations.

The tests performed in the laboratory setup considered, first, a given fixed reactive current reference, and, then, a current reference obtained by the algorithm to compensate load reactive power. In both cases the algorithm showed its capacity to correct the reference deviations caused by model parameter mismatches, improving the current tracking capability and, consequently, the supplied reactive power. Furthermore, since the impedances were being calculated online, the algorithm was also capable of correcting the references when equipment failure occurred, such as the loss of a capacitive cell from the capacitor bank.

The proposed algorithm is capable of estimating the HAPF branch parameters separately. Therefore, it is possible not only to obtain the needed impedances for the adaptation of the control references, but also to keep track of the capacitor bank capacitance. This feature may be used to identify faults in capacitive cells or to actively switch capacitors in and out of the capacitor bank to change the equipment's operating point, depending on the load reactive power demand, thereby effectively increasing the equipment's robustness, reliability and operation range for industrial applications.

Author Contributions: Conceptualization, S.C.F.; methodology, S.C.F. and R.B.G.; software, J.G.L.F.; validation, G.G.P.; investigation, J.G.L.F.; data curation, B.P.B.G.; writing—original draft preparation, S.C.F. and J.G.L.F.; writing—review and editing, R.B.G. and R.R.P.; supervision, R.R.P.; project administration, R.B.G. All authors have read and agreed to the published version of the manuscript.

Data Availability Statement: Not applicable.

Conflicts of Interest: The authors declare no conflict of interest.

Abbreviations

The following abbreviations are used in this manuscript:

ANF	Adaptive Notch Filter
APF	Active Power Filter
ARX	Auto-regressive Model with Exogenous Input
FCS-MPC	Finite Control Set Model Predictive Control
HAPF	Hybrid Active Power Filter
PCC	Point of Common Coupling
LMS	Least Mean Square
RLS	Recursive Least Square
SRF	Synchronous Reference Frame

References

1. Barva, A.V.; Joshi, S. A Comprehensive Survey on Hybrid Active Power Filter Topologies & Controller and Application in Microgrid. In Proceedings of the 2022 IEEE Region 10 Symposium (TENSYMP), Mumbai, India, 1–3 July 2022; pp. 1–6. [CrossRef]
2. Rodrigues Limongi, L.; Bradaschia, F.; Hermann de Oliveira Lima, C.; Cabral Cavalcanti, M. Reactive Power and Current Harmonic Control Using a Dual Hybrid Power Filter for Unbalanced Non-Linear Loads. *Energies* **2018**, *11*, 1392. [CrossRef]
3. Gonzatti, R.B.; Ferreira, S.C.; da Silva, C.H.; Pereira, R.R.; Borges da Silva, L.E.; Lambert-Torres, G. Smart Impedance: A New Way to Look at Hybrid Filters. *IEEE Trans. Smart Grid* **2016**, *7*, 837–846. [CrossRef]
4. Foster, J.G.L.; Pereira, R.R.; Gonzatti, R.B.; Sant'Ana, W.C.; Mollica, D.; Lambert-Torres, G. A Review of FCS-MPC in Multilevel Converters Applied to Active Power Filters. In Proceedings of the 2019 IEEE 15th Brazilian Power Electronics Conference and 5th IEEE Southern Power Electronics Conference (COBEP/SPEC), Santos, Brazil, 1–4 December 2019; pp. 1–6. [CrossRef]

5. Ferreira, S.C.; Gonzatti, R.B.; Pereira, R.R.; da Silva, C.H.; da Silva, L.E.B.; Lambert-Torres, G. Finite Control Set Model Predictive Control for Dynamic Reactive Power Compensation With Hybrid Active Power Filters. *IEEE Trans. Ind. Electron.* **2018**, *65*, 2608–2617. [CrossRef]

6. Foster, J.G.; Pereira, R.R.; Gonzatti, R.B.; Guimaraes, B.P.; Pinheiro, G.G.; Sant'ana, W.C. FCS-MPC Applied to Multilevel Hybrid Active Power Filter for Reactive Power and Harmonics Compensation. In Proceedings of the 2021 Brazilian Power Electronics Conference (COBEP), Joao Pessoa, Brazil, 7–10 November 2021; pp. 1–8. [CrossRef]

7. Yaramasu, V.; Rivera, M.; Wu, B.; Rodriguez, J. Model Predictive Current Control of Two-Level Four-Leg Inverters—Part I: Concept, Algorithm, and Simulation Analysis. *IEEE Trans. Power Electron.* **2013**, *28*, 3459–3468. [CrossRef]

8. Young, H.A.; Perez, M.A.; Rodriguez, J. Analysis of Finite-Control-Set Model Predictive Current Control With Model Parameter Mismatch in a Three-Phase Inverter. *IEEE Trans. Ind. Electron.* **2016**, *63*, 3100–3107. [CrossRef]

9. Wang, Y.; Wang, C.; Zeng, W.; Bai, F. Multifactorial Prediction Errors Analysis and a Feedback Self-Correction on Model Predictive Control for the Three-Phase Inverter. *IEEE Trans. Ind. Electron.* **2019**, *66*, 3647–3654. [CrossRef]

10. Wang, Y.; Liu, F.; Chen, S.; Shen, G.; Wang, Q.G. Prediction Errors Analysis and Correction on FCS-MPC for the Cascaded H-Bridge Multilevel Inverter. *IEEE Trans. Ind. Electron.* **2022**, *69*, 8264–8273. [CrossRef]

11. Liu, X.; Qiu, L.; Rodríguez, J.; Wu, W.; Ma, J.; Peng, Z.; Wang, D.; Fang, Y. Data-Driven Neural Predictors-Based Robust MPC for Power Converters. *IEEE Trans. Power Electron.* **2022**, *37*, 11650–11661. [CrossRef]

12. Heydari, R.; Young, H.; Rafiee, Z.; Flores-Bahamonde, F.; Savaghebi, M.; Rodriguez, J. Model-Free Predictive Current Control of a Voltage Source Inverter based on Identification Algorithm. In Proceedings of the IECON 2020 The 46th Annual Conference of the IEEE Industrial Electronics Society, Singapore, 18–21 October 2020; pp. 3065–3070. [CrossRef]

13. Li, Z.; Wang, B.; Wang, P.; Han, Y.; Garcia, C.; Rodriguez, J. Dynamic Forgetting Factor Based Bias-Compensated RLS Model Free Predictive Current Control for Voltage Source Inverter. In Proceedings of the 2022 IEEE 17th Conference on Industrial Electronics and Applications (ICIEA), Chengdu, China, 16–19 December 2022; pp. 195–200. [CrossRef]

14. Panten, N.; Hoffmann, N.; Fuchs, F.W. Finite Control Set Model Predictive Current Control for Grid-Connected Voltage-Source Converters With LCL Filters: A Study Based on Different State Feedbacks. *IEEE Trans. Power Electron.* **2016**, *31*, 5189–5200. [CrossRef]

15. Long, B.; Zhu, Z.; Yang, W.; Chong, K.T.; Rodríguez, J.; Guerrero, J.M. Gradient Descent Optimization Based Parameter Identification for FCS-MPC Control of LCL-Type Grid Connected Converter. *IEEE Trans. Ind. Electron.* **2022**, *69*, 2631–2643. [CrossRef]

16. Long, B.; Yang, W.; Hu, Q.; Guerrero, J.M.; Garcia, C.; Rodriguez, J.; Chong, K.T. Moth–Flame-Optimization-Based Parameter Estimation for FCS-MPC-Controlled Grid-Connected Converter with LCL Filter. *IEEE J. Emerg. Sel. Top. Power Electron.* **2022**, *10*, 4102–4114. [CrossRef]

17. Heydari, R.; Young, H.; Flores-Bahamonde, F.; Vaez-Zadeh, S.; González-Castaño, C.; Sabzevari, S.; Rodríguez, J. Model-Free Predictive Control of Grid-Forming Inverters With *LCL* Filters. *IEEE Trans. Power Electron.* **2022**, *37*, 9200–9211. [CrossRef]

18. Chen, X.; Wu, W.; Gao, N.; Liu, J.; Chung, H.S.H.; Blaabjerg, F. Finite Control Set Model Predictive Control for an LCL-Filtered Grid-Tied Inverter with Full Status Estimations under Unbalanced Grid Voltage. *Energies* **2019**, *12*, 2691. [CrossRef]

19. Widrow, B.; Glover, J.; McCool, J.; Kaunitz, J.; Williams, C.; Hearn, R.; Zeidler, J.; Eugene Dong, J.; Goodlin, R. Adaptive noise cancelling: Principles and applications. *Proc. IEEE* **1975**, *63*, 1692–1716. [CrossRef]

20. Ferreira, S.C.; Pereira, R.R.; Gonzatti, R.B.; da Silva, C.H.; da Silva, L.E.B.; Lambert-Torres, G.; Pereira, R.M.R. Adaptive notch filters: Comparison and applications in power conditioning. In Proceedings of the IECON 2014—40th Annual Conference of the IEEE Industrial Electronics Society, Dallas, TX, USA, 29 October–1 November 2014; pp. 1194–1200. [CrossRef]

21. Ferreira, S.C.; Gonzatti, R.B.; Silva, C.H.; da Silva, L.E.B.; Pereira, R.R.; Lambert-Torres, G. Adaptive Real-time Power Measurement Based on IEEE Standard 1459–2010. *Electr. Power Compon. Syst.* **2015**, *43*, 1307–1317. [CrossRef]

22. Pereira, R.R.; da Silva, C.H.; da Silva, L.E.B.; Lambert-Torres, G.; Pinto, J.O.P. New Strategies for Application of Adaptive Filters in Active Power Filters. *IEEE Trans. Ind. Appl.* **2011**, *47*, 1136–1141. [CrossRef]

23. Kouro, S.; Perez, M.A.; Rodriguez, J.; Llor, A.M.; Young, H.A. Model Predictive Control: MPC's Role in the Evolution of Power Electronics. *IEEE Ind. Electron. Mag.* **2015**, *9*, 8–21. [CrossRef]

24. Scoltock, J.; Geyer, T.; Madawala, U. Model Predictive Direct Current Control for a grid-connected converter: LCL-filter versus L-filter. In Proceedings of the 2013 IEEE International Conference on Industrial Technology (ICIT), Cape Town, South Africa, 25–28 February 2013; pp. 576–581. [CrossRef]

25. Falkowski, P.; Sikorski, A. Finite Control Set Model Predictive Control for Grid-Connected AC–DC Converters With LCL Filter. *IEEE Trans. Ind. Electron.* **2018**, *65*, 2844–2852. [CrossRef]

26. Cortes, P.; Rodriguez, J.; Silva, C.; Flores, A. Delay Compensation in Model Predictive Current Control of a Three-Phase Inverter. *IEEE Trans. Ind. Electron.* **2012**, *59*, 1323–1325. [CrossRef]

27. Mai-Van, C.; Duong-Minh, S.; Tran-Huu, D.; Binh-Pho, B.; Vu, P. An improved method of model predictive current control for multilevel cascaded H-bridge inverters. *J. Electr. Eng.* **2021**, *72*, 1–11. [CrossRef]

28. Li, H.; Liu, Y.; Yang, J. A Novel FCS-MPC Method of Multi-Level APF Is Proposed to Improve the Power Quality in Renewable Energy Generation Connected to the Grid. *Sustainability* **2021**, *13*, 4094. [CrossRef]

29. Young, H.A.; Marin, V.A.; Pesce, C.; Rodriguez, J. Simple Finite-Control-Set Model Predictive Control of Grid-Forming Inverters With LCL Filters. *IEEE Access* **2020**, *8*, 81246–81256. [CrossRef]

30. Ozkan, G.; Hoang, P.H.; Ramezani Badr, P.; Edrington, C.S.; Papari, B. Real-time thermal management for two-level active rectifier with finite control set model predictive control. *Int. J. Electr. Power Energy Syst.* **2021**, *131*, 107057. [CrossRef]

31. Vazquez, S.; Zafra, E.; Aguilera, R.P.; Geyer, T.; Leon, J.I.; Franquelo, L.G. Prediction Model With Harmonic Load Current Components for FCS-MPC of an Uninterruptible Power Supply. *IEEE Trans. Power Electron.* **2022**, *37*, 322–331. [CrossRef]

32. Ramírez, R.O.; Baier, C.R.; Espinoza, J.; Villarroel, F. Finite Control Set MPC with Fixed Switching Frequency Applied to a Grid Connected Single-Phase Cascade H-Bridge Inverter. *Energies* **2020**, *13*, 5475. [CrossRef]

33. Dahono, P. A control method to damp oscillation in the input LC filter. In Proceedings of the 2002 IEEE 33rd Annual IEEE Power Electronics Specialists Conference, Cairns, Australia, 23–27 June 2002; Proceedings (Cat. No. 02CH37289); Volume 4, pp. 1630–1635. [CrossRef]